Applied Physics Letters

AlGaN/GaN metal–insulator–semiconductor high electron mobility transistors (MISHEMTs) using plasma deposited BN as gate dielectric

Cite as: Appl. Phys. Lett. **118**, 072102 (2021); https://doi.org/10.1063/5.0027885
Submitted: 01 September 2020 . Accepted: 26 January 2021 . Published Online: 17 February 2021

Tsung-Han Yang, Jesse Brown, Kai Fu, Jingan Zhou, Kevin Hatch, Chen Yang, Jossue Montes, Xin Qi, Houqiang Fu, Robert J. Nemanich, Yuji Zhao, et al.

COLLECTIONS

Paper published as part of the special topic on Ultrawide Bandgap Semiconductors

ARTICLES YOU MAY BE INTERESTED IN

Suppression of the regrowth interface leakage current in AlGaN/GaN HEMTs by unactivated Mg doped GaN layer
Applied Physics Letters **118**, 072103 (2021); https://doi.org/10.1063/5.0034584

MBE growth and donor doping of coherent ultrawide bandgap AlGaN alloy layers on single-crystal AlN substrates
Applied Physics Letters **118**, 092101 (2021); https://doi.org/10.1063/5.0037079

Heavily Si-doped pulsed sputtering deposited GaN for tunneling junction contacts in UV-A light emitting diodes
Applied Physics Letters **118**, 072101 (2021); https://doi.org/10.1063/5.0040500

© 2021 Author(s).

Applied Physics Letters ARTICLE scitation.org/journal/apl

AlGaN/GaN metal–insulator–semiconductor high electron mobility transistors (MISHEMTs) using plasma deposited BN as gate dielectric

Cite as: Appl. Phys. Lett. **118**, 072102 (2021); doi: 10.1063/5.0027885
Submitted: 1 September 2020 · Accepted: 26 January 2021 ·
Published Online: 17 February 2021

View Online

Export Citation

CrossMark

Tsung-Han Yang,[1] Jesse Brown,[2] Kai Fu,[1] Jingan Zhou,[1] Kevin Hatch,[2] Chen Yang,[1] Jossue Montes,[1] Xin Qi,[1] Houqiang Fu,[3,a)] Robert J. Nemanich,[2,a)] and Yuji Zhao[1,a)]

AFFILIATIONS

[1]School of Electrical, Computer, and Energy Engineering, Arizona State University, Tempe, Arizona 85282, USA
[2]Department of Physics, Arizona State University, Tempe, Arizona 85282, USA
[3]Department of Electrical and Computer Engineering, Iowa State University, Ames, Iowa 50011, USA

Note: This paper is part of the Special Topic on Ultrawide Bandgap Semiconductors.
[a)]**Authors to whom correspondence should be addressed:** houqiang@iastate.edu; robert.nemanich@asu.edu; and Yuji.Zhao@asu.edu

ABSTRACT

AlGaN/GaN metal–insulator–semiconductor high electron mobility transistors (MISHEMTs) were fabricated on Si substrates with a 10 nm boron nitride (BN) layer as a gate dielectric deposited by electron cyclotron resonance microwave plasma chemical vapor deposition. The material characterization of the BN/GaN interface was investigated by X-ray photoelectric spectroscopy (XPS) and UV photoelectron spectroscopy. The BN bandgap from the B1s XPS energy loss is ~5 eV consistent with sp^2 bonding. The MISHEMTs exhibit a low off-state current of 1×10^{-8} mA/mm, a high on/off current ratio of 10^9, a threshold voltage of −2.76 V, a maximum transconductance of 32 mS/mm at a gate voltage of −2.1 V and a drain voltage of 1 V, a subthreshold swing of 69.1 mV/dec, and an on-resistance of 12.75 Ω·mm. The interface state density (D_{it}) is estimated to be less than 8.49×10^{11} $cm^{-2}eV^{-1}$. Gate leakage current mechanisms were investigated by temperature-dependent current–voltage measurements from 300 K to 500 K. The maximum breakdown electric field is no less than 8.4 MV/cm. Poole–Frenkel emission and Fowler–Nordheim tunneling are indicated as the dominant mechanisms of the gate leakage through the BN gate dielectric at low and high electric fields, respectively.

Published under license by AIP Publishing. https://doi.org/10.1063/5.0027885

III-Nitride-based semiconductors have recently attracted considerable interest due to their superior high-power and high-frequency performances compared with Si, GaAs, or other compound semiconductors.[1,2] AlGaN/GaN high electron mobility transistors (HEMTs) are considered as next-generation power switching devices due to the existence of a polarization-induced two-dimensional electron gas (2DEG) at the AlGaN/GaN interface.[3–5] Nevertheless, the performance of conventional Schottky-gate HEMTs has been limited by the high leakage current and low forward bias.[6] As a result, metal–insulator–semiconductor high electron mobility transistors (MISHEMTs) with gate dielectrics serve an effective solution to overcome the leakage current and surface issues of conventional Schottky-gate HEMTs.[7–9] Various dielectric materials have been investigated for the AlGaN/GaN MISHEMTs, including SiO_2,[10] Si_3N_4,[10–12] Al_2O_3,[9] and some other high-k dielectrics.[13,14] However, the performance of the AlGaN/GaN MISHEMTs is still far from its theoretical limitation because of strong coulomb scattering at the dielectric/AlGaN interface. Moreover, interface states and border traps result in reliability issues such as hysteresis effects in device performance.[15] It is of critical importance to seek better gate dielectric materials for AlGaN/GaN MISHEMTs.

Compared to oxide-based gate dielectric materials, nitride-based materials have significant advantages due to the lack of Ga–O-related interface traps. Previous reports studied silicon nitride-based gate dielectric MISHEMTs,[11,16–18] where gate leakage, gate swing, and interface trap density are still remaining issues to be addressed. Recently, ultra-wide bandgap (UWBG) semiconductor boron nitride (BN) has garnered considerable research interest for high power and high temperature applications[19–21] due to its ultra-wide bandgap of ~5.2 eV,[22] projected high breakdown electrical field of 12 MV/cm,

Published under license by AIP Publishing

relatively large dielectric constant of 3.76,[23] and high thermal conductivity of 1300 W/K m. In addition, BN exists in various crystalline forms including a-BN (amorphous), h-BN (hexagonal), c-BN (cubic), and w-BN (wurtzite). Among all these forms, hexagonal boron nitride is the most stable one. Since gallium nitride is also a hexagonal structure, if we are looking for a perfect dielectric layer for gallium nitride, then h-BN should be a more promising candidate over other nitride-based dielectric materials.

BN exists in the sp^3-bonded cubic phase analogous to diamond and the sp^2-bonded hexagonal phase analogous to graphite or graphene. BN has also been formed in disordered films that include mixtures of sp^2 and sp^3 bonding.[24] Recently, some researchers demonstrated BN as a gate dielectric in diamond-based or gallium oxide-based field effect transistors,[25–27] where the BN thin film was transferred via mechanical exfoliation. However, there are a few reports on BN as a gate dielectric for AlGaN/GaN MISHEMTs.[7,28,29] In this work, we have demonstrated AlGaN/GaN MISHEMTs with electron cyclotron resonance microwave plasma chemical vapor deposition (ECR-MPCVD) deposited BN as a gate dielectric. The ECR-MPCVD process used here is carbon free. *In situ* X-ray photoelectric spectroscopy (XPS) and UV photoelectron spectroscopy (UPS) are used to characterize the BN thin film structure and the BN/GaN cap interface band offset. The transfer and output characteristics of AlGaN/GaN MISHEMTs indicate excellent switching performance with a high on/off ratio of 10^9 and a subthreshold swing of 69.1 mV/dec. Gate leakage mechanisms under low and high electric fields are also investigated.

The AlGaN/GaN MISHEMT epitaxial layers were grown by metalorganic chemical deposition (MOCVD) on 6-in. Si substrates. The Al, Ga, and N sources are trimethylaluminum (TMAl), trimethylgallium (TMGa), and ammonia (NH_3), respectively. SiH_4 was used as an n-type dopant and H_2 was the carrier gas. The structure consists of a 3 nm GaN cap layer, followed by a 28 nm AlGaN barrier layer, a 1 nm AlN interlayer, a 0.23 μm n-GaN layer, and a 3.6 μm unintentionally doped GaN buffer layer. A 10 nm BN thin film layer was deposited as a gate dielectric on AlGaN/GaN MISHEMTs by electron cyclotron resonance microwave plasma chemical vapor deposition (ECR-MPCVD) with a base pressure of 3×10^{-9} Torr. Before deposition, the AlGaN/GaN MISHEMT wafer was first cleaned in the deposition chamber by flowing 35 sccm of N_2 and 20 sccm of H_2 at a pressure of 2×10^{-4} Torr at 875 °C for 60 min with N_2 flow while heating and cooling. The sample surface was then characterized by *in situ* UPS and XPS shown in Figs. 1(c) and 1(a), respectively. BN was then deposited on the cleaned sample surface for 20 min with He of 36 sccm, Ar of 2.5 sccm, H_2 of 1 sccm, N_2 of 12.5 sccm, and BF_3 of 1 sccm. The sample was biased at −60 V. The deposition temperature was 850 °C, the microwave power was 1.4 kW, and the chamber pressure was 1×10^{-4} Torr with N_2 flow while heating and cooling. The sample cleaning and BN deposition parameters in ECR-MPCVD are summarized in Table I.

In situ XPS and UPS were used to analyze the sample surface before and after BN deposition. The x-ray source in XPS is monochromatic Al-Kα x rays with an energy of 1486 ± 0.2 eV. The UV source for UPS is a helium discharge lamp, where the He II emission line (40.8 eV) is used to measure the valence band maximum (VBM) of the clean AlGaN/GaN surface and the deposited BN layer. The chamber base pressure is 5×10^{-10} Torr monitored by a hot filament ion gauge. An Omicron Scientia R3000 spectrometer with a four-element electrostatic lens was used in a sweep mode to scan the full energy range of photoelectrons. The hemispherical analyzer has a slit size of 0.4 mm and a pass energy of 100 eV for XPS (2 eV for UPS), leading to an energy resolution of 150 meV for XPS (3 meV for UPS). It is worth noting that transition lifetime of core holes and thermal motion can cause peak broadening beyond the energy resolution. The spectrometer is calibrated using the gold 4f energy (for XPS) and the Fermi energy (for both XPS and UPS). The XPS spectra were fit with Gaussian functions. Peak centers correspond to the binding energy of element core level electrons. Peak areas are used to calculate relative concentrations of elements,[30] the thickness of the deposited layer,[31] and the ratio of sp^2:sp^3 hybridization[32] (i.e., the ratio of hexagonal to cubic BN). The bandgap of BN is measured using the boron electron energy loss peak.[30,33] UPS spectra were fit with a linear extrapolation to determine the VBM.

Figure 1(a) shows the full XPS energy range before and after BN deposition. No oxygen signal (∼532 eV) was observed after the cleaning process of the AlGaN/GaN MISHEMT wafer, indicating a clean AlGaN/GaN surface. The presence of the Al 2p peak is consistent with a GaN cap thickness of 3 nm over the AlGaN layer as the escape depth of the photoelectrons in GaN is about 10 nm. After the 20-min BN deposition, the Ga peaks were no longer visible. A small amount of fluorine is typically observed due to the residue from the boron precursor (BF_3). Figure 1(b) demonstrates the XPS spectrum of the boron 1s core level. The fraction of sp^2:sp^3 bonding was estimated using the π-plasmon:B 1s intensity ratio (green line:blue line). A reference film containing h-BN without any evidence of c-BN in Fourier transform inferred spectroscopy measurements was reported to have a π-plasmon:B 1s intensity ratio of 0.122 ± 0.018. The measured ratio of the deposited BN is 0.087 ± 0.020, indicating that the BN layer is mostly (71% ± 17%) in the hexagonal phase. Figure 1(c) presents the valence band spectrum using the He II photon source, and the VBM values for clean GaN and BN surfaces are 3.0 ± 0.03 eV and 3.4 ± 0.05 eV, respectively. Figure 1(d) presents the energy band alignment of BN deposited on the GaN cap surface. The bandgap of h-BN was found to be 5.0 ± 0.1 eV using the onset of the core level energy loss peak.

After the BN thin film deposition by ECR-MPCVD, conventional photolithography was utilized to fabricate the AlGaN/GaN MISHEMTs. Figure 2(a) shows a schematic of the AlGaN/GaN on the Si sample layer structure before BN deposition, and Figs. 2(b)–2(g) present the device fabrication process flow. The samples were first cleaned using acetone and isopropyl alcohol in an ultrasonic bath and then rinsed with de-ionized water. Then, the mesa was defined and etched by chlorine-based inductively coupled plasma-reactive ion etching (ICP-RIE). Next, the dielectric via hole for source and drain contacts was etched by SF_6-based ICP-RIE, which selectively etches the h-BN at a rate of 48 nm/min without reacting with the GaN underneath. It is important to use proper etching methods since over-etching of the BN thin film through the GaN cap layer is unwanted.[34] After mesa etching, photolithography and lift-off processes were used to define the source and drain contacts. A 30 s oxygen plasma treatment was applied to remove residual photoresist, followed by a 30 s soaking in diluted hydrochloric acid (HCl) to remove potential surface oxidization layers. The Ti/Al/Ni/Au (20/120/30/100 nm) metal stacks were deposited by electron beam evaporation for source and drain

Published under license by AIP Publishing

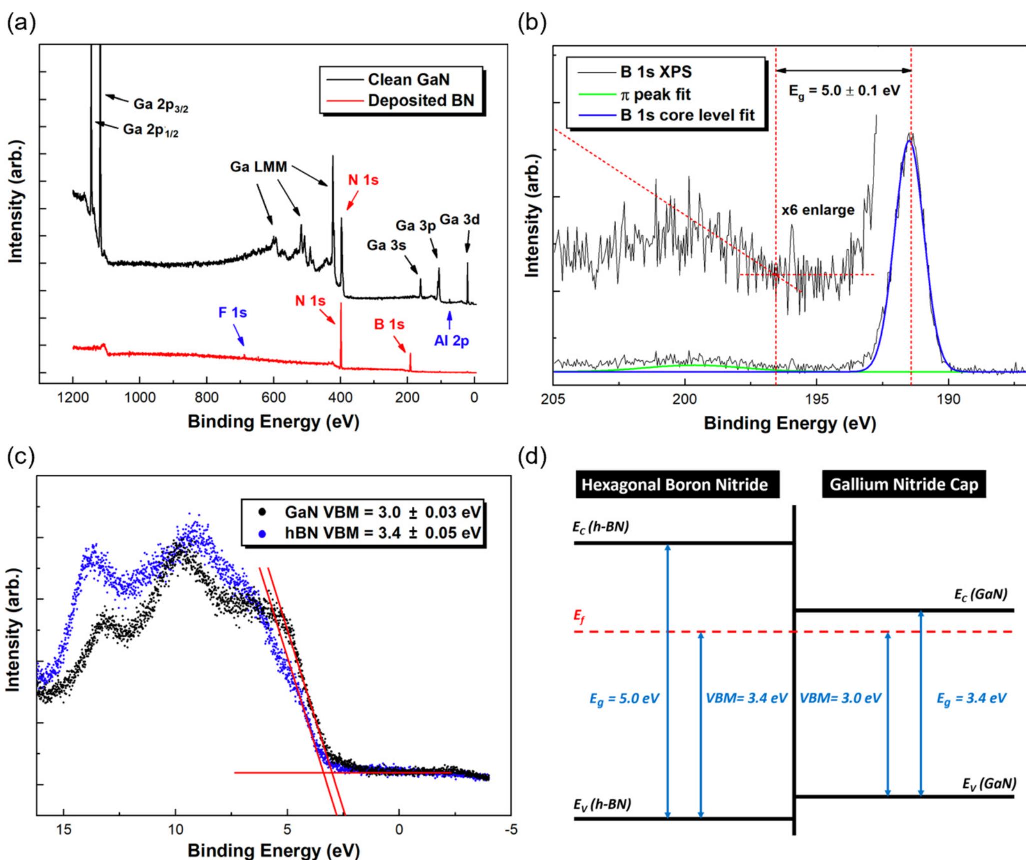

FIG. 1. (a) Full XPS energy range before and after deposition of boron nitride. No significant signal from oxygen or carbon on the clean GaN. (b) XPS boron 1s core level (191.5 eV). The π peak (green line) to core level ratio indicates that the BN layer is mostly (70%–80%) in the hexagonal sp^2 structure. The onset of the π peak indicates a bandgap of 5.0 ± 0.1 eV. The boron to nitrogen ratio is B:N = 0.9. (c) Valence band spectrum using the He II photon source. The valence band maximum for clean GaN and BN surfaces is 3.0 ± 0.03 eV and 3.4 ± 0.05 eV relative to the Fermi level, respectively. (d) Energy band alignment of BN deposited on GaN using the measure values of the VBM and bandgap of the BN layer.

TABLE I. The cleaning and deposition conditions for the BN/AlGaN/GaN HEMTs.

	Cleaning	Deposition
Substrate temperature	875 ± 25 °C	825 ± 25 °C
Chamber pressure	2×10^{-4} Torr	2×10^{-4} Torr
Applied bias	N/A	−60 W
Microwave power	N/A	1400 W
Time	60 min	20 min
Gas flow (sccm)		
He	0	35
Ar	0	2.5
N_2	35	12.5
BF_3	0	1
H_2	20	1

metal contacts, followed by a rapid thermal annealing (RTA) at 850 °C under an ambient nitrogen atmosphere. Finally, after defining the gate metal pattern by photolithography, the Ni/Au gate metal stacks were deposited on the BN gate dielectric by electron beam evaporation. The gate width (W_G), gate length (L_G), gate source distance (L_{GS}), and gate drain distance (L_{GD}) are 500 μm, 4 μm, 4 μm, and 4 μm, respectively. The corresponding metal–insulator–semiconductor (MIS) diodes were also fabricated for J_g–V_g characterization.

The basic DC characteristics of the BN/AlGaN/GaN MISHEMTs were first investigated. Figure 3(a) demonstrates the transfer characteristics of the devices. The maximum drain current is about 62.6 mA/mm at $V_{DS} = 1$ V and $V_{GS} = 0$ V, and the threshold voltage is about −2.76 V. The maximum transconductance ($g_{m,\,max}$) is about 32 mS/mm when $V_{DS} = 1$ V and $V_{GS} = -2.1$ V. The devices exhibit a small subthreshold swing of 69.1 mV/dec and a high I_{on}/I_{off} ratio on the order of 10^9. The effective interface state density D_{it} can be estimated by the subthreshold swing equation:[29]

$$SS = \frac{kT}{q}\ln(10)\left(1 + \frac{C_s + C_{it}}{C_{ox}}\right),$$

Published under license by AIP Publishing

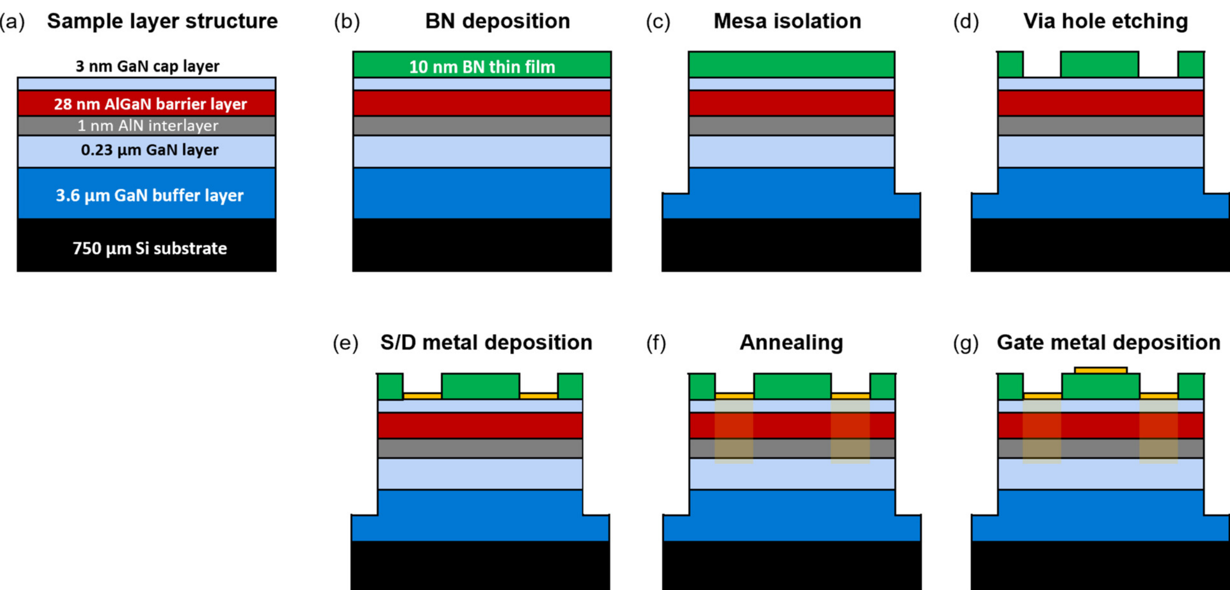

FIG. 2. The fabrication process of the BN/AlGaN/GaN HEMTs. (a) AlGaN/GaN on the Si sample layer structure. (B) 10 nm boron nitride thin film deposition by ECR-MPCVD as the gate dielectric. (c) Mesa isolation through chlorine-based ICP etching. (d) Gate dielectric via hole for drain and source contacts through SF6-based ICP etching. (e) Source and drain metal contact deposition by e-beam evaporation. The lift-off method is applied. (f) Rapid thermal annealing for the Ohmic contact formation. (g) Gate metal contact deposition by e-beam evaporation.

where C_s, C_{it}, and C_{ox} are the semiconductor capacitance, interface state-induced capacitance, and dielectric capacitance, respectively. While the semiconductor capacitance C_s varies nontrivially with the applied gate, it is still possible to estimate the maximum D_{it} by the equation below:[11]

$$D_{it} = \frac{C_{it}}{q} < C_{ox}\left(\frac{qSS}{kT\ln(10)} - 1\right).$$

Since the relative dielectric constant of BN is ~3.76,[23] the maximum D_{it} can thus be calculated to be $\sim 8.49 \times 10^{11}\ \mathrm{cm^{-2}\ eV^{-1}}$. Figure 3(b) demonstrates output characteristics of the devices under forward sweeping and backward sweeping. The V_{DS} is swept from 0 V to 5 V (black line) and 5 V to 0 V (red dashed line) with V_{GS} stepped between −2 V and 1 V with steps of 0.5 V. No obvious differences were observed in the two output curves, indicating a very low hysteresis effect. The on-resistance is about 12.75 Ω·mm.

In order to investigate the gate dielectric properties, the gate leakage–gate voltage (I_G–V_G) curve was measured as shown in Fig. 4(a), where the drain voltage and source voltage are set as 0 V. A very low gate leakage current of 10^{-8} mA/mm was observed,

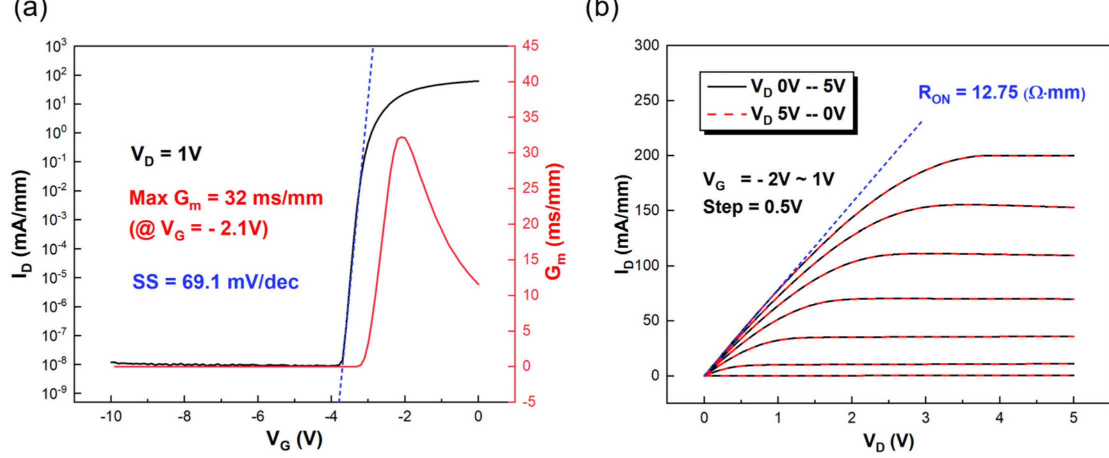

FIG. 3. (a) (Black) Transfer curve of the BN/AlGaN/GaN MISHEMTs at $V_{DS} = 1$ V on a semi-log scale at room temperature. (Red) Transconductance of the device on a linear scale at room temperature. The maximum G_m is about 32 mS/mm at $V_G = -2.1$ V. The subthreshold swing is about 69.1 mV/dec. (b) Output characteristics of the BN/AlGaN/GaN MISHEMTs, where V_{GS} swept from −2 V to 1 V with a step of 0.5 V on a linear scale. The on-resistance is about 12.75 Ω·mm by linear extraction.

Published under license by AIP Publishing

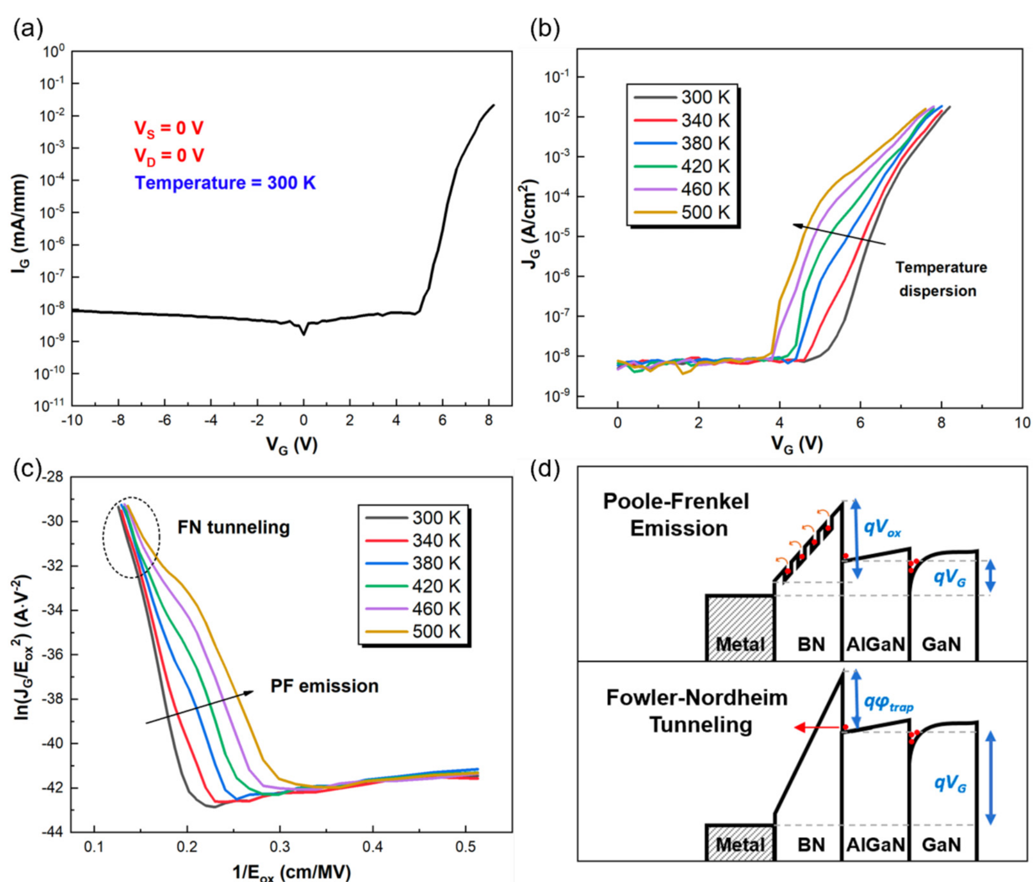

FIG. 4. (a) I_G–V_G curve of the ECR-MPCVD-BN/AlGaN/GaN MISHEMTs. The gate leakage current is of 10^{-7} mA/mm range or less under both reverse and low forward gate voltages. (b) J_G–V_G curves of devices at various temperatures from 300 K to 500 K with a step of 40 K. (c) FN plots at various temperatures. At a relatively low electric field, PF emission dominates the leakage current, which results in an obvious temperature dispersion. At a high electric field, FN tunneling dominates the leakage current, and the curves merged again since they are no longer temperature dependent. (d) Schematic energy band diagrams of PF emission and FN tunneling.

suggesting good insulating properties of the BN gate dielectric. Due to the gate current compliance setting, the MISHEMTs were not able to be stressed to forward hard breakdown, but the corresponding electric-field maximum can still be estimated from Fig. 4(a) to be >8.4 MV/cm,[11] which is not far from the theoretical breakdown electric field of BN (12 MV/cm). Conventional Schottky gate HEMTs with the same device structure were also fabricated as reference devices. Table II shows the comparison of device performances for BN MISHEMTs, conventional Schottky gate HEMTs, and other reported MISHEMTs with different dielectrics.[9,11,12] Our fabricated devices (BN MISHEMTS and conventional Schottky gate HEMTs) showed similar on-resistance and maximum transconductance. However, the off-state gate leakage current of BN MISHEMTs was three orders lower than that of conventional Schottky gate HEMTs. Compared with reported MISHEMTs from Refs. 9,11, and 12, the on-resistance of our device is slightly higher, which results in a lower transconductance, possibly due to the unoptimized Ohmic contact process. Although the breakdown electric field of BN is lower than that of SiN_x and SiO_2, the BN brings a lower gate leakage at a thinner thickness.

To further investigate the gate leakage mechanism, Fig. 4(b) presents temperature-dependent gate current density vs gate voltage (J_G–V_G) curves of the MIS diode from 300 K to 500 K. The MIS diode has a diameter of 200 μm and an area of 3.14×10^{-4} cm^2. When V_G <3.8 V, the gate leakage current is very small and below the setup lower limit (Agilent 4330). When 3.8 V < V_G < 7 V, the curves exhibit an obvious temperature-related dispersion, which indicates that a certain thermal emission mechanism plays an important role here. When V_G >7 V, the curves at different temperatures began to merge again. There are some widely accepted mechanisms for the gate leakage through the dielectric, such as Poole–Frenkel (PF) emission, trap-assisted tunneling, Fowler–Nordheim (FN) tunneling, and space charge limited current.[35] A more in-depth leakage mechanism analysis can be studied from the Fowler–Nordheim plot [FN plot, $\ln(J_G/E_{ox})$ vs $E_{ox}{}^{1/2}$]. The electric field across the BN dielectric (E_{ox}) can be calculated from the below equations:

$$E_{ox} = \frac{V_{ox}}{t_{ox}},$$

$$V_{ox} = V_G + \frac{1}{q}(\Delta E_{c1} - \Delta E_{c2}),$$

$$\Delta E_{c2} = \varphi_{Ni} - \chi_{ox},$$

Published under license by AIP Publishing

TABLE II. The device performance comparison of BN MISHEMTs, conventional Schottky gate HEMTs, and other reported MISHEMTS using different dielectrics.[9,11,12]

Gate dielectric	Thickness (nm)	R_{on} (Ω·mm)	G_m (mS/mm)	Reverse I_g (mA/mm)	E_{br} (MV/cm)	
Schottky gate	N/A	13.76	36	$\sim 10^{-5}$	1	This paper
BN	10	12.75	32	$\sim 10^{-8}$	>8.4	This paper
Si_3N_4	20	6.7	N/A	$\sim 10^{-7}$	14	Ref. 11
Si_3N_4	20	2.88	75	$\sim 10^{-8}$	13.3	Ref. 12
Al_2O_3	16	5.4	100	$\sim 10^{-7}$	5	Ref. 9

where V_{ox}, t_{ox}, φ_{Ni}, χ_{ox}, and ΔE_{c1} are the voltage across the dielectric, dielectric thickness (10 nm), Ni work function (5.15 eV),[36] dielectric electron affinity (4.5 eV), and band offset between the BN/GaN interface, respectively. An iterative calculation method was conducted to extract the value of ΔE_{c1}. Further details can be found in Ref. 11. Figure 4(c) shows the FN plot of the devices from 300 K to 500 K. When the electric field is low ($0.15 < 1/E_{ox} < 0.3$), the curves were strongly dependent on temperature, suggesting that the PF emission is the dominant leakage mechanism. At a high electric field ($1/E_{ox} < 0.15$), the curves are independent of temperature, indicating that FN tunneling dominates the gate leakage. Figure 4(d) illustrates the schematic energy band diagram of these two dominant leakage current mechanisms. At low electric fields, when the temperature increased, the thermal excitation of electrons may emit from traps into the conduction band of the dielectric, hence the leakage current increased. At high electric fields, when the dielectric barrier is thin enough, the electron wave function may penetrate through the triangular potential barrier tunneling directly from the AlGaN to the metal.

In summary, we have demonstrated an AlGaN/GaN MISHEMT structure with ECR-MPCVD-grown BN as a gate dielectric. *In situ* XPS and UPS were used for comprehensive surface characterization. The *in situ* high temperature cleaning and deposition processes lead to a high quality BN dielectric film. The devices exhibit a low off-state current of 10^{-8} mA/mm, a high on/off current ratio of 10^9, a stable threshold voltage of -2.76 V, a high maximum transconductance of 32 mS/mm, a nearly ideal subthreshold swing of 69.1 mV/dec, and an on-resistance of 12.75 Ω·mm. The interface state density (D_{it}) is estimated to be less than 8.49×10^{11} cm^{-2} eV^{-1}. The maximum breakdown electric field is no less than 8.4 MV/cm. The leakage current mechanisms were also studied by temperature-dependent measurements. Poole–Frenkel emission and Fowler–Nordheim tunneling are two dominant mechanisms for the leakage current under low and high electric fields, respectively. These results can serve as important references for future studies on BN-based gate dielectrics for GaN power devices.

This work was supported in part by the ARPA-E PNDIODES Program monitored by Dr. Isik Kizilyalli under Grant No. DE-AR0000868 and in part by the NASA HOTTech Program under Grant No. 80NSSC17K0768. This work was also supported as part of ULTRA, an Energy Frontier Research Center funded by the U.S. Department of Energy (DOE), Office of Science, Basic Energy Sciences (BES), under Award No. DE-SC0021230. We acknowledge the use of facilities within the Eyring Materials Center at Arizona State University. The device fabrication was performed at the ASU NanoFab, which was supported by NSF Contract No. ECCS-1542160.

DATA AVAILABILITY

The data that support the findings of this study are available within the article.

REFERENCES

[1] H. Amano, Y. Baines, E. Beam, M. Borga, T. Bouchet, P. R. Chalker, M. Charles, K. J. Chen, N. Chowdhury, R. Chu, C. De Santi, M. M. De Souza, S. Decoutere, L. Di Cioccio, B. Eckardt, T. Egawa, P. Fay, J. J. Freedsman, L. Guido, O. Häberlen, G. Haynes, T. Heckel, D. Hemakumara, P. Houston, J. Hu, M. Hua, Q. Huang, A. Huang, S. Jiang, H. Kawai, D. Kinzer, M. Kuball, A. Kumar, K. B. Lee, X. Li, D. Marcon, M. März, R. McCarthy, G. Meneghesso, M. Meneghini, E. Morvan, A. Nakajima, E. M. S. Narayanan, S. Oliver, T. Palacios, D. Piedra, M. Plissonnier, R. Reddy, M. Sun, I. Thayne, A. Torres, N. Trivellin, V. Unni, M. J. Uren, M. Van Hove, D. J. Wallis, J. Wang, J. Xie, S. Yagi, S. Yang, C. Youtsey, R. Yu, E. Zanoni, S. Zeltner, and Y. Zhang, J. Phys. D **51**(16), 163001 (2018).
[2] J. A. del Alamo, Nature **479**(7373), 317 (2011).
[3] X. Liu, H. Gu, K. Li, L. Guo, D. Zhu, Y. Lu, J. Wang, H.-C. Kuo, Z. Liu, and W. Liu, AIP Adv. **7**(9), 095305 (2017).
[4] K. J. Chen and C. Zhou, Phys. Status Solidi A **208**(2), 434 (2011).
[5] R. S. Pengelly, S. M. Wood, J. W. Milligan, S. T. Sheppard, and W. L. Pribble, IEEE Trans. Microwave Theory Tech. **60**(6), 1764 (2012).
[6] Z. Yatabe, J. T. Asubar, and T. Hashizume, J. Phys. D **49**(39), 393001 (2016).
[7] J.-C. Gerbedoen, A. Soltani, M. Mattalah, M. Moreau, P. Thevenin, and J.-C. De Jaeger, Diamond Relat. Mater. **18**(5-8), 1039 (2009).
[8] M. Van Hove, S. Boulay, S. R. Bahl, S. Stoffels, X. Kang, D. Wellekens, K. Geens, A. Delabie, and S. Decoutere, IEEE Electron Device Lett. **33**(5), 667 (2012).
[9] P. D. Ye, B. Yang, K. K. Ng, J. Bude, G. D. Wilk, S. Halder, and J. C. M. Hwang, Appl. Phys. Lett. **86**(6), 063501 (2005).
[10] K. Geng, D. Chen, Q. Zhou, and H. Wang, Electronics **7**(12), 416 (2018).
[11] M. Hua, C. Liu, S. Yang, S. Liu, K. Fu, Z. Dong, Y. Cai, B. Zhang, and K. J. Chen, IEEE Trans. Electron Devices **62**(10), 3215 (2015).
[12] Z. Zhang, G. Yu, X. Zhang, X. Deng, S. Li, Y. Fan, S. Sun, L. Song, S. Tan, and D. Wu, IEEE Trans. Electron Devices **63**(2), 731 (2016).
[13] C. Liu, E. F. Chor, and L. S. Tan, Semicond. Sci. Technol. **22**(5), 522 (2007).
[14] M. Kanamura, T. Ohki, T. Kikkawa, K. Imanishi, T. Imada, A. Yamada, and N. Hara, IEEE Electron Device Lett. **31**(3), 189 (2010).
[15] G. Meneghesso, G. Verzellesi, F. Danesin, F. Rampazzo, F. Zanon, A. Tazzoli, M. Meneghini, and E. Zanoni, IEEE Trans. Device Mater. Reliab. **8**(2), 332 (2008).
[16] Z. Tang, Q. Jiang, Y. Lu, S. Huang, S. Yang, X. Tang, and K. J. Chen, IEEE Electron Device Lett. **34**(11), 1373 (2013).
[17] J.-Y. Shiu, V. Desmaris, N. Rorsman, K. Kumakura, T. Makimoto, H. Zirath, and E. Y. Chang, Semicond. Sci. Technol. **22**(7), 717 (2007).
[18] X. Wang, S. Huang, Y. Zheng, K. Wei, X. Chen, G. Liu, T. Yuan, W. Luo, L. Pang, and H. Jiang, IEEE Electron Device Lett. **36**(7), 666 (2015).
[19] J. Lee, T.-J. Ha, K. N. Parrish, S. F. Chowdhury, L. Tao, A. Dodabalapur, and D. Akinwande, IEEE Electron Device Lett. **34**(2), 172 (2013).
[20] S. K. Jang, J. Youn, Y. J. Song, and S. Lee, Sci. Rep. **6**, 30449 (2016).
[21] J. Eichler and C. Lesniak, J. Eur. Ceram. Soc. **28**(5), 1105 (2008).

Published under license by AIP Publishing

[22]G. Cappellini, G. Satta, M. Palummo, and G. Onida, Phys. Rev. B **64**(3), 035104 (2001).
[23]A. Laturia, M. L. Van de Put, and W. G. Vandenberghe, npj 2D Mater. Appl. **2**(1), 6 (2018).
[24]R. J. Nemanich, S. A. Solin, and R. M. Martin, Phys. Rev. B **23**(12), 6348 (1981).
[25]J. Bae, H. W. Kim, I. H. Kang, G. Yang, and J. Kim, Appl. Phys. Lett. **112**(12), 122102 (2018).
[26]Y. Sasama, K. Komatsu, S. Moriyama, M. Imura, S. Sugiura, T. Terashima, S. Uji, K. Watanabe, T. Taniguchi, and T. Uchihashi, Phys. Rev. Mater. **3**(12), 121601 (2019).
[27]J. Kim, M. A. Mastro, M. J. Tadjer, and J. Kim, ACS Appl. Mater. Interfaces **9**(25), 21322 (2017).
[28]T. Q. Nguyen, H.-A. Shih, M. Kudo, and T.-K. Suzuki, Phys. Status Solidi C **10**(11), 1401 (2013).
[29]B. Ren, M. Liao, M. Sumiya, J. Li, L. Wang, X. Liu, Y. Koide, and L. Sang, J. Alloys Compd. **829**, 154542 (2020).
[30]J. Shammas, T. Sun, F. A. M. Koeck, A. Rezikyan, and R. J. Nemanich, Diamond Relat. Mater. **56**, 13 (2015).
[31]A. Jablonski and J. Zemek, Surf. Interface Anal. **41**(3), 193 (2009).
[32]J. Shammas, Y. Yang, X. Wang, F. A. M. Koeck, M. R. McCartney, D. J. Smith, and R. J. Nemanich, Appl. Phys. Lett. **111**(17), 171604 (2017).
[33]H. Nohira, W. Tsai, W. Besling, E. Young, J. Pétry, T. Conard, W. Vandervorst, S. De Gendt, M. Heyns, and J. Maes, J. Non-Cryst. Solids **303**(1), 83 (2002).
[34]S. Grenadier, J. Li, J. Lin, and H. Jiang, J. Vac. Sci. Technol. A **31**(6), 061517 (2013).
[35]F.-C. Chiu, Adv. Mater. Sci. Eng. **2014**, 1.
[36]N. Miura, T. Nanjo, M. Suita, T. Oishi, Y. Abe, T. Ozeki, H. Ishikawa, T. Egawa, and T. Jimbo, Solid-State Electron. **48**(5), 689 (2004).

Published under license by AIP Publishing